J. Astrophys. Astr. (June 2017) 38:29
DOI 10.1007/s12036-017-9448-7

Review

Soft X-ray Focusing Telescope Aboard AstroSat: Design, Characteristics and Performance

K. P. SINGH[1,*], G. C. STEWART[2], N. J. WESTERGAARD[3], S. BHATTACHARAYYA[1], S. CHANDRA[1], V. R. CHITNIS[1], G. C. DEWANGAN[4], A. T. KOTHARE[1], I. M. MIRZA[1], K. MUKERJEE[1], V. NAVALKAR[1], H. SHAH[1], A. F. ABBEY[2], A. P. BEARDMORE[2], S. KOTAK[1], N. KAMBLE[1], S. VISHWAKARAMA[1], D. P. PATHARE[1], V. M. RISBUD[1], J. P. KOYANDE[1], T. STEVENSON[2], C. BICKNELL[2], T. CRAWFORD[2], G. HANSFORD[2], G. PETERS[2], J. SYKES[2], P. AGARWAL[5], M. SEBASTIAN[5], A. RAJARAJAN[5], G. NAGESH[6], S. NARENDRA[6], M. RAMESH[6], R. RAI[6], K. H. NAVALGUND[6], K. S. SARMA[6], R. PANDIYAN[6], K. SUBBARAO[6], T. GUPTA[7], N. THAKKAR[7], A. K. SINGH[7] and A. BAJPAI[1]

[1]Tata Institute of Fundamental Research, Homi Bhabha Road, Mumbai 400 005, India.
[2]Department of Physics and Astronomy, University of Leicester, Leicester, United Kingdom.
[3]Technical University of Denmark, National Space Institute, Copenhagen, Denmark.
[4]Inter University Centre for Astronomy & Astrophysics, Pune 411 007, India.
[5]Vikram Sarabhai Space Centre, Thiruvananthapuram 695 022, India.
[6]ISRO Satellite Centre, Bengaluru 560 017, India.
[7]Space Application Centre, Ahmedabad 380 015, India.
*Corresponding author. E-mail: singh@tifr.res.in

MS received 9 November 2016; accepted 30 January 2017; published online 19 June 2017

Abstract. The Soft X-ray focusing Telescope (SXT), India's first X-ray telescope based on the principle of grazing incidence, was launched aboard the AstroSat and made operational on October 26, 2015. X-rays in the energy band of 0.3–8.0 keV are focussed on to a cooled charge coupled device thus providing medium resolution X-ray spectroscopy of cosmic X-ray sources of various types. It is the most sensitive X-ray instrument aboard the AstroSat. In its first year of operation, SXT has been used to observe objects ranging from active stars, compact binaries, supernova remnants, active galactic nuclei and clusters of galaxies in order to study its performance and quantify its characteriztics. Here, we present an overview of its design, mechanical hardware, electronics, data modes, observational constraints, pipeline processing and its in-orbit performance based on preliminary results from its characterization during the performance verification phase.

Keywords. Space vehicles: instruments—instrumentation: detectors.

1. Introduction

AstroSat, the first Indian space observatory, carries a number of co-pointed telescopes and detectors to observe a cosmic source simultaneously in a wide band of X-rays (0.3–100 keV) and in visible light, near ultraviolet, and far ultraviolet radiations. It was launched by the Indian Space Research Organisation (ISRO) on 28 September 2015 at 10:00 IST and placed into a circular orbit of 650 kms above the Earth at an inclination of 6° and orbital period of 98 min. The several instruments onboard the AstroSat are: three Large Area Xenon Proportional Counters (LAXPCs), a Soft X-ray focusing Telescope (SXT), two UV Imaging Telescopes (UVIT), a Cadmium-Zinc Telluride Imager (CZTI), a Scanning Sky Monitor (SSM), and a Charged Particle Monitor (CPM). A description of the principal instruments onboard AstroSat, their pre-launch specifications and capabilities, is given in Singh *et al.* (2014).

SXT has been designed to provide soft X-ray images and spectra in the energy range of 0.3–8.0 keV by focusing X-rays on to a cooled Charge Coupled Device (CCD). Based on the principle of grazing incidence in a conical approximation of the Wolter I geometry, it is capable of providing imaging, spatially resolved spectroscopy and variability observations of cosmic sources.

The soft X-ray coverage, combined with the wide-band coverage of the hard X-ray instruments addresses many scientific problems such as the detection of black-body components, partial or complete absorption in all types of X-ray binaries with compact accretors like white dwarfs, neutron stars and black holes and in active galactic nuclei (AGN). The spectral resolution of the CCD allows us to find low energy hot plasma components and their attendant line emission in active stars, supernova remnants, and the hot intra-cluster gas, and study the physics of shocks and accretion disks, coronae, photo-ionized regions and their density, temperature, ionization degree, and elemental abundances.

Here, we give an overview of the SXT[1], and its scientific capabilities based on a preliminary post-launch evaluation of its characteristics. This paper is organized as follows. In section 2 and section 3, we discuss the overall instrument configuration and the optics respectively. The detectors and electronics are discussed in section 4 and section 5 respectively. Observational constraints are discussed in section 6 followed by the details of the pipeline processing and products in section 7. The in-orbit operations carried out and the performance of SXT showing its scientific capabilities are given in section 8. Further details of the post-launch calibration will be published elsewhere.

2. Configuration

A photograph of the fully assembled SXT is shown in Fig. 1 and a schematic of the SXT is shown in Fig. 2. SXT has a focal length of 2 meters and geometric area of $\sim$250 cm^2. The X-rays are focused on a CCD in the focal plane camera assembly. The CCD is cooled by a thermoelectric cooler (TEC) connected via a cold finger and a heat pipe to a radiator plate. The radiator plate is always facing the dark side of the satellite and is being maintained at a temperature in the range of -48°C to -60°C. The CCD is being maintained at a temperature in the range of -81°C to -85°C after launch.

3. X-ray optics assembly

The overall design of the optics, the development and testing of mirrors and the assembly of the mirrors for the SXT was carried out at the Tata Institute of Fundamental Research and a brief description is given here. The optics assembly of X-ray reflecting mirrors is housed in a tubular structure made of CFRP (carbon fibre reinforced plastic) developed at the Vikram Sarabhai Space

[1]More details about the SXT can be found at http://AstroSat-ssc.iucaa.in/

Figure 1. The fully assembled SXT before integration with the satellite.

Centre. A deployable door at the top end of the telescope covered the optical elements protecting them from contamination before launch. This was deployed 2 weeks after launch, in a one time operation, and is perched at an angle of 256°. A thermal baffle lies between the door and the mirror assembly made of anodized aluminium alloy 6061 T6. The baffle protects the telescope from the Sun, and provides a base for mounting the heaters to maintain the optics specified to be within 17 ± 5°C. The Sun avoidance angle with the thermal baffle is -45°. A forward tube of CFRP covers the thermal baffle assembly and 1α section (see below) of the mirrors assembly. Several rings and rear tube of CFRP provide an interface between the middle flange of the optics to the FPCA (Focal Plane Camera Assembly). The entire telescope is held at its centre of gravity by a Deck Interface Ring (DIR) made of Al alloy 6061. There is a

Figure 2. A schematic of the SXT showing the complete assembly of all the components of the SXT.

Charge Coupled Device (CCD) in the FPCA at the common focus of all the mirrors in order to image the cosmic sources. A schematic of the SXT is shown in Fig. 2.

The SXT optics consists of a set of coaxial and confocal shells of conical mirrors approximating paraboloidal and hyperboloidal shapes and arranged behind each other in Wolter I geometry. X-rays are first reflected by internally reflecting paraboloidal (1α section) mirrors and then reflected to the prime focus of the telescope by internally reflecting hyperboloid (3α section) mirrors. At grazing incidence, the active region of the mirror is just a thin annulus giving a small collecting area even for a large diameter mirror. Thus nesting of Wolter I shells is incorporated to improve the filling factor of the circle defined by the outermost shell. Higher nesting is achieved by using shells made of very thin mirror elements. SXT has 40 complete shells of thin foils (0.2 mm thickness) of aluminium with replicated gold surfaces on the reflecting side for each section. Each shell consists of four quadrants, therefore, there are a total of 320 mirrors. Each mirror is 100 mm long. The radius of the outermost shell is 130 mm, while that of the innermost shell is 65 mm. The focal length of the telescope is 2000 mm measured from the middle of the two sections. The design is based on that described in Westergaard *et al.* (1990) and Kunieda *et al.* (2001). The mirrors were tested and evaluated extensively using X-ray reflectivity measurements as described in Sagdeo *et al.* (2010). The mirrors showed roughness of ∼7–10 Å.

3.1 *On-axis effective area and vignetting*

The on-axis effective area of the telescope has been calculated based on simulations of the telescope after incorporating the latest reflection coefficients for the gold and a scattering function matched to the point spread function (see below) as determined from observations of point sources. The on-axis effective area of the telescope including transmission through the thin filter but excluding the CCD Quantum Efficiency (QE) is shown in Fig. 3. The area is also corrected for photons scattered by the PSF of the optics outside a radius of 12 arcmin from the central optical axis on the CCD.

4. Focal plane camera assembly

The FPCA containing a thermo-electrically cooled CCD was built by the Space Research Centre of the Department of Physics and Astronomy at the University of Leicester, UK and is based on the mechanical and

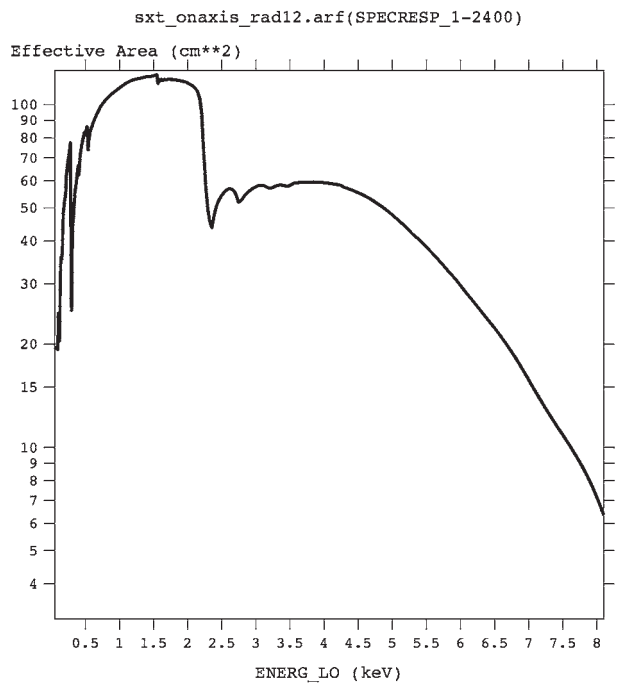

Figure 3. On-axis effective area of SXT at various energies. Only the filter transmission is included here but not the QE of the CCD. A radius of 12 arcmin is used for the collection of photons incident on the CCD from a point source. The effective area is maximum between 1 and 2 keV.

electrical design used successfully for the XRT on the Swift satellite (Burrows *et al.* 2005) with some changes to account for the shorter focal length of the SXT and to the proton shield which could have a reduced mass due to the more benign orbit. At the heart of the FPCA is the X-ray sensitive CCD, where the photons from the optics are focused. The health and the operational conditions required for the CCD to detect and accurately measure the energy of X-rays include a vacuum, low temperature and protection from optical light contamination. To reduce long-term deterioration of the CCD performance, protection from the in-orbit energetic particle background is also required. Therefore in addition to the basic cryostat vacuum chamber containing the detector, the CCD is coupled to a thermo-electric cooler (TEC) to bring the detector to its operating temperature of about −82°C in addition to a passively cooling radiator system (large cold plate kept in the night/cold side of the orbit). The radiator plate provides a base cold-finger temperature of at least −45°C (or colder) and is connected to a cold finger via an ethane-filled heat pipe, and the TEC is mounted on the cold finger. The TEC can give a further maximum temperature differential of 40°C thus cooling the CCD further. At the entrance window to the detector is an optical blocking filter. Surrounding the CCD detector is the proton shield. To monitor the performance of the CCD detector and its associated processing electronics radioactive fluorescent sources (at the 4 corners of the detector and on the FPCA door) are also provided. A schematic of the FPCS mechanical assembly is shown in Fig. 4.

4.1 *Optical blocking filter*

A thin Luxel filter is installed in front of the CCD to block optical light while minimizing the loss off soft X-ray sensitivity. The filter is similar to that used in the Swift XRT and consists of a single fixed polyimide film ∼1800 Å thick, coated on one side with ∼500 Å of aluminium. The optical transmission is about 2.5×10^{-3}.

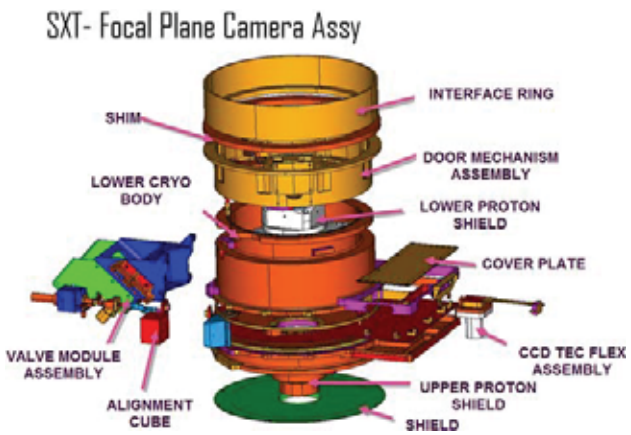

Figure 4. The FPCA and its various components.

4.2 *The CCD*

The CCD used is the CCD-22 MOS device supplied to the University of Leicester produced by e2V Technologies Inc., UK, and with a heritage of use in the XMM-Newton and the Swift observatories. It has the following characteristics:

(1) A three-phase frame transfer.
(2) An open electrode structure and a depletion depth of ∼30 microns giving a useful band pass of 0.2 to 10 keV.
(3) An imaging area of 610 × 602 array of 40 × 40 micron square pixels including over-scan. In astronomical operation this gives an imaging field of view of 600 × 600 pixels each ∼4 arc sec square for the SXT optics focal length of 2.0 m. The sky region imaged is circular with a radius of ∼20 arcminutes with the corners of the field of view used for the calibration sources.
(4) A storage region of 600 × 602 array of pixels with each pixel of 38 × 12 micron pitch.

4.3 *Quantum efficiency*

The quantum efficiency of the CCD was measured at the University of Leicester and modelled using a Monte Carlo approach with a physically realistic model of the CCD. The open-gate structure and the depletion depth gives good sensitivity over the energy range of ∼0.2–10 keV. The details will be discussed in a forthcoming paper which will also include a detailed discussion of the energy resolution and overall performance of the camera. The quantum efficiency for both isolated and single pixel events is shown in Fig. 5.

4.4 *Gain and energy resolution*

Five ^{55}Fe radioactive calibration sources are mounted in the camera for in-flight calibration at energies of 5.895 keV (Mn-Kα) and 6.49 keV (Mn-Kβ). These two lines interact with the silicon in the CCD and produce two escape peaks at 4.16 and 4.75 keV respectively. Fluorescence lines are due to Al, Si, Cl and TI at 1.49, 1.74, 2.62 and 4.51 keV respectively and serve as secondary calibrators. Four corner sources illuminate areas of the

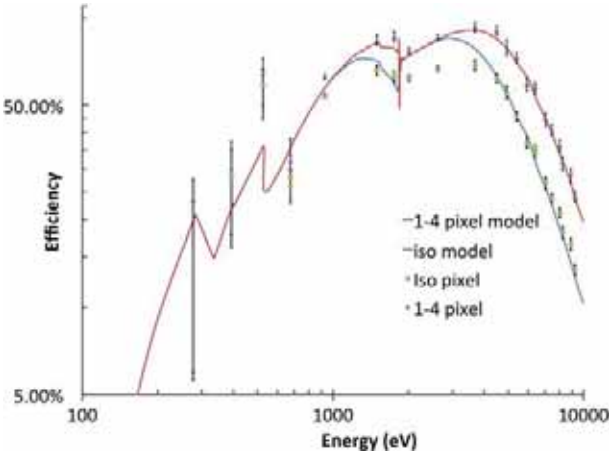

Figure 5. The quantum efficiency of the CCD.

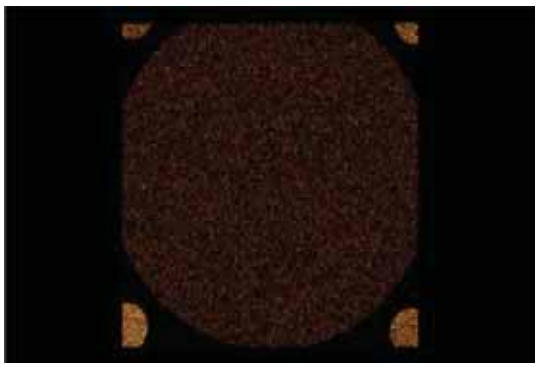

Figure 6. In-flight image of corner and door calibration sources prior to door opening.

CCD outside the circular Field-of-View (FoV) defined by the optical blocking filter. The fifth source mounted on the cryostat door facing the CCD is no longer available following the deployment of the door which was permanently opened on October 26, 2015. An image of the calibration sources taken in orbit after launch is shown in Fig. 6. The calibration source data are used in orbit to determine

(1) the gain and energy scale for the ADC output of the electronics. The zero point of the energy scale is taken from the bias offset noise peak .
(2) a measure of the energy resolution of the detector and the read-out noise of the electronics system.
(3) the charge transfer inefficiency of the CCD.

Ground calibration measurements of a number of monochromatic X-ray sources using a low noise laboratory electronics system were also made to determine the energy resolution of the CCD and its energy dependence to inform the Monte Carlo modelling process discussed above.

5. The processing electronics

The SXT processing electronics (PE) housed in a separate box consists of ten cards of circuits (EL-01 to -08, EL-3A, Motherboard), including three Field Programmable Gate Arrays (FPGAs). During the CCD 'readout' the electrons from each pixel capacitor are transferred out of the imaging array to a readout array where the voltage caused by the charge accumulation is sampled and converted into a digital number (the number of Analog-Digital Units or ADUs), using an Analogue to Digital Converter (ADC). The science data and the bias map data from the CCD are passed on to the EL-03, where the analog to digital conversion happens. The science data are then stored in a memory (M1) in EL-05 via the first FPGA (EL-04). This memory has two portions: upper and lower. When the first FPGA stores the data in the upper memory, the second FPGA (EL-06) takes the previous set of data from the lower portion of memory M1. Next, when the first FPGA stores in the lower portion of memory M1, the second FPGA takes from the upper portion of memory M1. This way data are continuously passed on from the first FPGA to the second FPGA. For bias map generation, a separate dedicated mode can be enabled which sends the entire CCD frame in 24 s. In the second FPGA, the data are packaged in 2 Kb blocks (see below), and passed on to the third FPGA (EL-07). Here the data are sent to the satellite memory (allocated for SXT) via high bit rate telemetry (HBT; rate is 4 MHz). The housekeeping (HK) data from the FPCA are passed on to the third FPGA via EL-3A, and eventually sent to the satellite memory via Low-Bit rate Telemetry (LBT; rate is 40 kHz). The power from the satellite interface is supplied to various cards via the relay card (EL-02) and the DC–DC tray (EL-01). The input of the DC–DC tray is between 28 V and 42 V, and its output to each card is a regulated voltage. The tele-commands from the satellite interface are passed on to the various cards, and eventually to the FPCA via EL-3A and EL-02.

5.1 *Data acquisition modes*

SXT data can be acquired in several modes by commanding the CCD. The different modes are based on the observers' requirements. The main mode used for regular observations is the Photon Counting mode (PC) that covers the entire FoV and is the default mode for observations; a Photon Counting Window mode (PCW) with 5 pre-defined windows centred on the CCD; a Fast (or Timing) mode (FM) in which only the central 150×150 pixels of the CCD are read out and can be useful for

observing very strong cosmic sources to avoid pile-up; a Bias Map mode (BM), and a calibration mode (CM) reading from four small windows in the corners (each of size $= 80 \times 80$ pixels) and a central 100×100 window. X-ray spectral information is available in all the modes, and the time resolution in the PC, PCW, CM modes is 2.4 s and 0.278 s in the FM mode. An energy threshold is applied to the events recorded in the PC, FW and PCW modes before storing the data.

All data (Level 1) in each mode are packaged in 2K blocks. However, the content of a 2K block is not the same for all the modes. For the PC, PCW and FW modes (i.e., the science data), only the channel number above the pre-selected threshold is stored in the 2K block along with the pixel coordinate and the CCD frame identification. These data are stored in the 15–2042 bytes of the total of 2048 bytes of a 2K block. Three bytes are required to store each of (a) CCD frame identification, (b) CCD row number of the pixel and threshold value and (c) CCD column number of the pixel and the channel number. The 1–14 bytes (header) and 2043–2048 bytes (footer) store the 2K block number, mode information, on-board time, window location and numbers to check the validity of the 2K block. More details of the PE can be found in Kothare *et al.* (2009).

6. Observational constraints

There are several pointing constraints on the SXT observations, primarily to protect the CCD, the optical blocking filter above the CCD, and the mirror coating. The most important one is the Sun avoidance angle (>45°) and is absolutely essential for the safety of the SXT. The other constraints that can affect the data quality are the 'Earth limb' or the 'bright Earth' avoidance angle, the satellite RAM avoidance angle (angle between the view axis of the satellite and the direction of motion or the velocity vector of the satellite), and the Moon avoidance angle. The RAM angle avoidance of >12° is applied by the mission operations for all the observations as a lower angle can affect the mirrors.

The bright Earth avoidance angle of $\geq 110°$ is used in the SXT pipeline while converting Level 1 data to Level 2 data products. The Moon avoidance angle is not being used at the moment.

The SXT and the UVIT and LAXPC instruments are not exactly co-aligned. Sources appear along the central axis of the SXT only if the SXT is chosen as the prime instrument by an observer. Since the SXT is always ON, and has a large field-of-view of 40 arcmin, it observes all sources even when it is the secondary instrument of observation. The source position on the CCD is determined by the offset between the SXT and the other instruments. This is ∼6 arcmin between SXT and UVIT, for example.

7. Pipeline processing and products

Control of the overall AstroSat spacecraft as well as data down link from all scientific instruments is carried out from the ISRO Telemetry, Tracking and Command Network (ISTRAC) located at Bengaluru. The data from the different payloads are segregated and then sent for processing at the Payload Operation Centres (POC) for individual payloads and the higher level data generated by the POC are archived by Indian Space Science Data Centre (ISSDC) located at Bylalu. The Payload Operation Centre (POC) for the SXT is located at the Tata Institute of Fundamental Research, Mumbai.

The POC processes all the 'Level 1' data received from ISSDC to create astronomer-friendly 'Level 2' products using the SXT pipeline software. The pipeline requires Level-1 data files and calibration data files from SXT calibration database, CALDB as inputs for its execution. The complete data processing is done in a single chain by a single command to generate Level-2 data products. The data processing steps involve event extraction using SXTEVTGEN, time tagging of events using SXTTIMETAG, coordinate transformation from raw to detector and XY co-ordinates using SXTCOORD, bias subtraction and adjustment using SXTBIASSUB and SXTBIASADJ, flagging of bad pixels and calibration source events using SXTFLAGPIX, events grading and PHA construction for each event using SXTEVTGRADE, search for hot and flicker pixels using SXTHOTPIX and then carrying out PHA to PI conversion of events using SXTCALCIPI. The data processing thus generates an unfiltered event file. The tool SXTFILTER is used to create the Level-2 filter file known as the MKF file as it is produced by a program called 'make filter'. A cleaned event file is generated by running SXTSCREEN on unfiltered event file using this Level-2 MKF file, HK and event range files from the calibration database. Basic Level 2 data products such as an image, light curve and spectrum are generated utlising clean event file by product generation tool, SXT-PRODUCTS, designed based on XSELECT interface from HEASARC (NASA). The Level-2 data products so generated using pipeline processing are further processed and corrected for the exposure time. The target source centroid position can be determined

with associated errors using SXTCENTRIOD. The SXTMKARF uses the simulated area of the telescope for different extraction regions on the CCD frame and generates corrected Area Response Function (ARF) and includes the transmission through the thin filter, and also accounts for vignetting, point spread function and exposure correction based on an exposure map. The exposure map is generated using SXTEXPOMAP, which accounts for the loss of flux due to marked *bad* pixels and columns. The products are stored in FITS files compatible with the HEASoft package[2]. This package includes tools like XRONOS for timing analysis, XIMAGE for image analysis, and XSPEC can be used with the corrected ARF, detector response matrix (RMF) along with the spectral data to fit spectral models to the data and to understand the intrinsic source spectrum. The light curve and image are also corrected for exposure using the exposure map. Processed Level 2 data are validated by the POC and uploaded to ISSDC, where they can be downloaded by the proposers. As per AstroSat policy, data remain private for a period of one year from the date of observation, after which they are publicly accessible from the ISSDC website[3].

Various calibration files required for data processing are stored in the standard CALDB format. The SXT processing pipeline, CALDB files, and sample data are all available in the 'Data and Analysis' section of the the AstroSat Science Support Cell website, http://AstroSat-ssc.iucaa.in.

8. In-orbit operations and performance

The processing electronics for the SXT was switched on September 30, 2015. The House Keeping (HK) information, e.g., the CCD voltages, the camera door pressure, the vacuum level inside the camera, the temperatures of the CCD and the cold finger connected to the radiator plate, the bit patterns of the data etc. were monitored on the Low-Bit Telemetry (LBT) stream. The optics temperature has been maintained on the average at $19.2°C \pm 0.5°C$ (1α section) and at $19.5°C \pm 1.0°C$ (3α section) under the various orientations of the satellite in the last one year. The health check was satisfactory and the high bit telemetry stream was also switched on and the CCD was put into the calibration mode. The venting operation was initiated on the same day in the following orbit to release the built up gases inside the camera. This venting operation, lasting for 10 min every day and the ultimate vacuum inside the camera was achieved on October 6th. The TEC was switched on and the temperature controller was commanded to hold the temperature of the CCD to $-82°C$ on October 8, 2015 where it has been held till date. The CCD read-out mode was changed to the bias mode on October 10, 2015 and the integrity of the thin optical blocking filter was verified using an onboard LED. The CCD mode was changed back to the calibration mode on October 13, 2015 and the telescope door above the X-ray optics assembly was opened successfully on October 15, 2015. The CCD bias maps were obtained on October 25–26 until the opening of the camera door on October 26 when the mode was changed to the photon counting (PC) mode for first light. The bias mode and calibration mode data were used to characterise the low energy noise peak and the energy gain values, which were then used to set the low energy threshold for the PC, PCW and FW modes and to derive the PHA to energy conversion. The noise performance of the read-out electronics was calculated by fitting a Gaussian to the zero-point bias level and was found to be $\sim$7 electrons. The threshold level for the photon counting (PC) mode was based on this data and set to 120 ADUs, which is $\sim 4\sigma$ above the bias offset and applied to the data in the PC, PCW, FW modes. Currently the default setting onboard is 100 ADUs, as the bias offset peak or zero point has been found to be at 62 ADC channel since April 2016. The energy calibration from the corner sources (and the central source before October 26, 2015) is being obtained continuously and so far no change has been noticed in the gain and the peak positions. The gain and resolution obtained in flight are in agreement with the ground calibrations. The CCD temperature is holding steady between $-81.5°C$ to $-84.5°C$, the variation of 3°C observed being due to a large swing of temperature of the cold radiator plate that has been varying between $-50°C$ to $-65°C$, since the launch. No drifts have been observed so far in the CCD gain due to the temperature variations.

The PHA spectrum of the calibration sources post-launch is shown in Fig. 7. The spectral response matrix calculated previously has been used with XSPEC together with a model including delta functions at appropriate energies to fit the data to derive the gain function and confirm the spectral response matrix. The nominal resolution requirement of 150 eV at 6 keV is

[2]The HEASoft software suite is maintained by the High Energy Archive Science Research Center (HEASARC), and can be downloaded freely from http://heasarc.gsfc.nasa.gov/lheasoft/

[3]ISSDC website: http://issdc.gov.in/astro.html

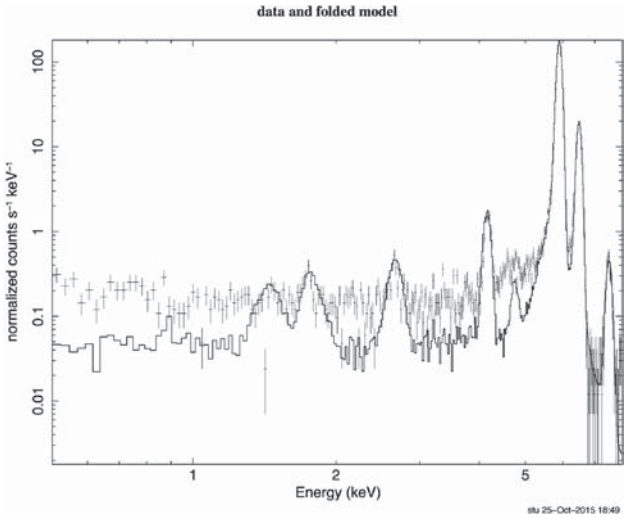

Figure 7. Fit of detector model to calibration spectrum.

met. A more detailed discussion of the CCD performance and its variation in time will be presented in a future paper.

The first six months of observations with AstroSat were dedicated for Performance Verification (PV) observations, followed by a six-month long guaranteed time (GT) observation phase and some of the preliminary results on the in-orbit performance were reported in Singh *et al.* (2016). Here we update and add to those results. In a typical orbit, the SXT data is not usable during any SAA passage, the eclipse of the source by the Earth, and when the bright Earth floods the available memory allocation with optical light. The net observing efficiency of the SXT varies from source to source but on the average is about 25%.

The SXT has observed several X-ray sources like PKS2155-304, Tycho SNR, 1E 0102-73.2 – a SNR, AB Dor – an active Sun-like star, A1795 – a cluster of galaxies, and several AGNs, etc. SXT was pointed such that 1E0102.2-7219 and PKS2155-304 were incident on different parts of the CCD to determine the bore-sight of the telescope and the vignetting in the SXT at different off-axis angles. Since PKS2155-304 is variable we have mostly relied on the use of the supernova remnant 1E0102.2-7219 in the small magellanic cloud which, however, required long observations, as the source is very weak in the SXT. This source emits mostly soft X-rays and is seen in 0.3–3 keV energy band. The results from these observations showed that the bore sight of the SXT is close to the centre of the FoV and the CCD detector coordinates at $X = 302 \pm 7$ and $Y = 285 \pm 7$ pixels. The vignetting of the telescope or the projected area as a function of off-axis angle was also determined.

X-ray image of a blazar, Mrk 501, a point source, obtained with the SXT is shown in Fig. 8. All images, spectra and analysis here are based on photon events of grades 0–12 (see for example, Romano *et al.* 2005), thus effectively removing all charge particles, and after removing the data taken during the passages though the South Atlantic Anomaly (SAA) using the inputs from the Charged Particle Monitor (CPM) (Rao *et al.* 2016) on AstroSat. The total count rate from Mrk 501 is 2.0±0.01 per sec in the energy range of 0.3–7.0 keV corresponding to source flux of $\sim 7 \times 10^{-11}$ ergs cm^{-2} s^{-1}. The on-axis Point Spread Function (PSF) in the focal plane has been determined from these observations of Mrk 501 and of other AGN observed in the PV and GT phase and are well characterized by a double King function. The two King functions have core radii of ∼50–60 and ∼700 arcsec respectively with the broader King function having ∼8% of the intensity compared to the narrower King function. The PSF has a FWHM (Full Width Half Maximum) of ∼100 arcsec while the half encircled energy radius is ∼5.5 arcmin (or Half Power Diameter, HPD is ∼11 arcmin). The off-axis PSF's and the energy dependence of the PSF are in the process of being determined. Care must be taken while carrying out the spectral analysis to include as much of the encircled energy as possible while extracting a spectrum and optimizing the background component simultaneously, and then use the corresponding response for the telescope area function from those provided. For very bright sources, the user may have to include a radius as large as 18 arcmins to get all the photons and then use background from a deep field with no detectable objects. Data from deep fields will be made available to the observers. Deep exposures of blank sky regions show that the total background in 0.3–7.0 keV and covering the entire FoV of the SXT's is ∼0.20 counts s^{-1}. For a typical detection radius of 6–10 arcmin on the CCD for a weak source, the background is ∼0.06 counts s^{-1}. Thus in a 10000 s exposure, the 5σ point source detection limit is ∼0.015 counts s^{-1} above the background, which roughly corresponds to 5.5×10^{-13} ergs cm^{-2} s^{-1} (∼12 μCrab). SXT images of extended sources like the supernova remnant Tycho and cluster of galaxies like A1795 are shown in Figs. 9 and 10.

In Fig. 11, we show our recent result from the joint analysis of SXT, Swift XRT (Burrows *et al.* 2005) and NuStar (Harrison *et al.* 2013) observations of Tycho supernova remnant. The spectra were fitted with a common spectral model having an absorbing column density of 9.5×10^{21} cm^{-2}, a bremsstrahlung component of kT = 0.26 keV, and Gaussian lines at 0.64, 1.85, 1.90, 2.24

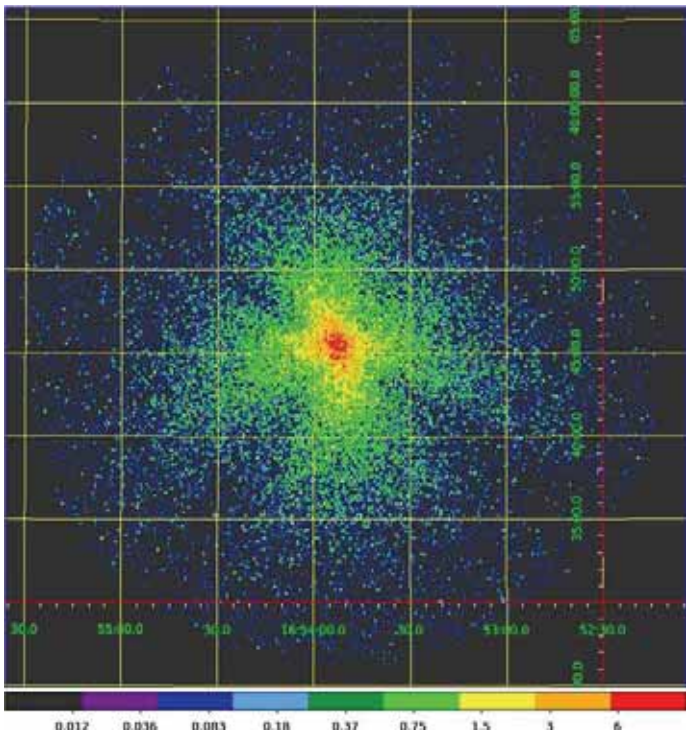

Figure 8. SXT image of Mrk 501.

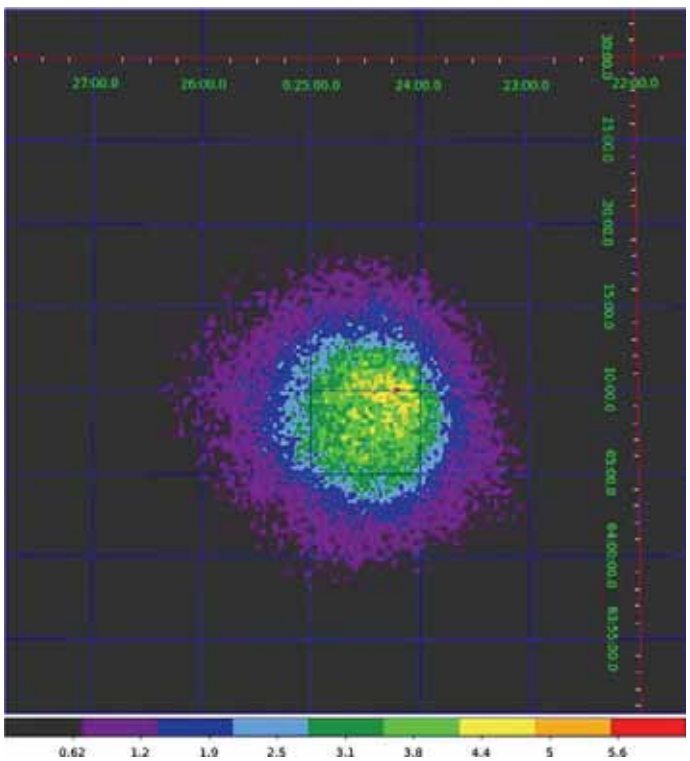

Figure 9. SXT image of Tycho supernova remnant showing the well known limb brightening on one side.

2.45, 2.99, 3.81 and 6.44 keV. The addition of the NuStar data required an additional cut-off power-law (very flat with photon index $= -0.56$) component with energy cutoff at 1.59 keV. The unfolded spectrum from all the instruments is also shown in the figure and displays a very good match from all the instruments. The SXT

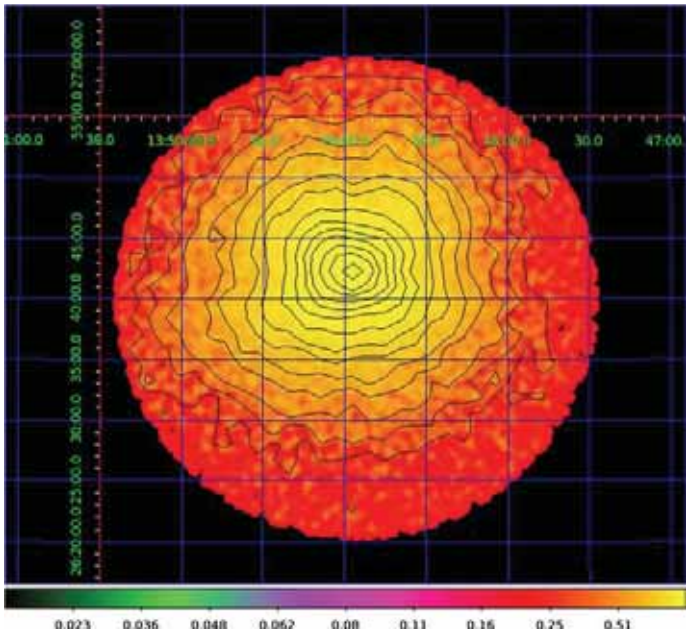

Figure 10. SXT image of Abell 1795 cluster of galaxies after a slight smoothing using a Gaussian function, sigma = 40 arcsec.

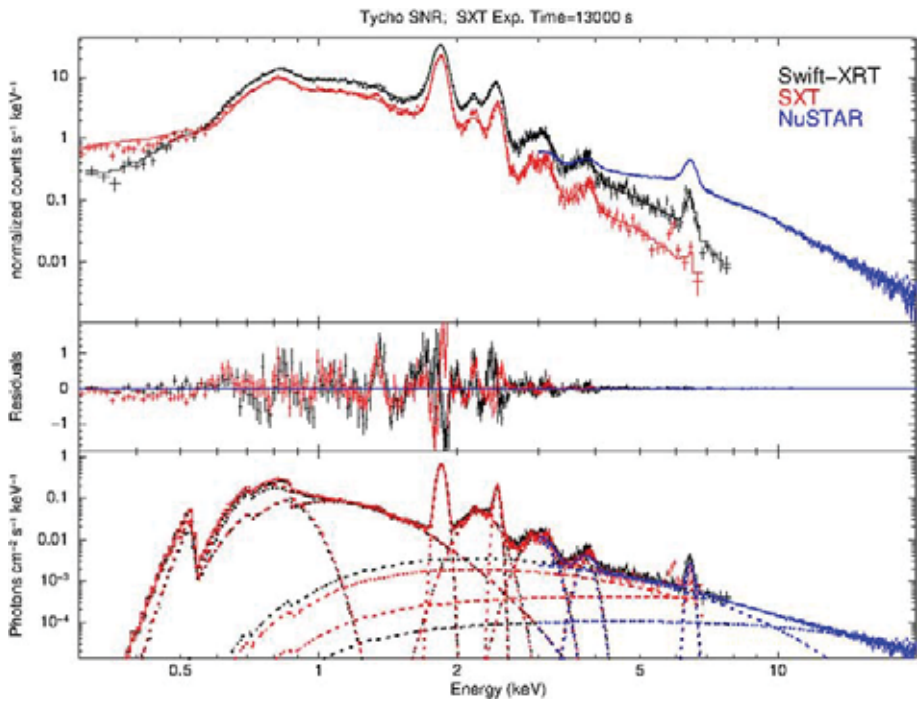

Figure 11. The X-ray spectrum of Tycho SNR as obtained with the SXT, Swift XRT and the NuStar and fitted with a common ad-hoc model with all parameters frozen to the same values obtained from the Swift XRT observation (*upper panel*). The *middle panel* shows the residuals from the fit, and the *bottom panel* shows the unfolded spectrum, with the dotted lines showing the contributions of each component.

spectrum of E0102.2-7219 fitted with the model developed by the International Astronomical Consortium for High Energy Calibration (IACHEC) (Plucinsky *et al.* 2016) is shown in Fig. 12. These results show a good consistency with other instruments and the good quality of X-ray spectra that can be obtained with SXT.

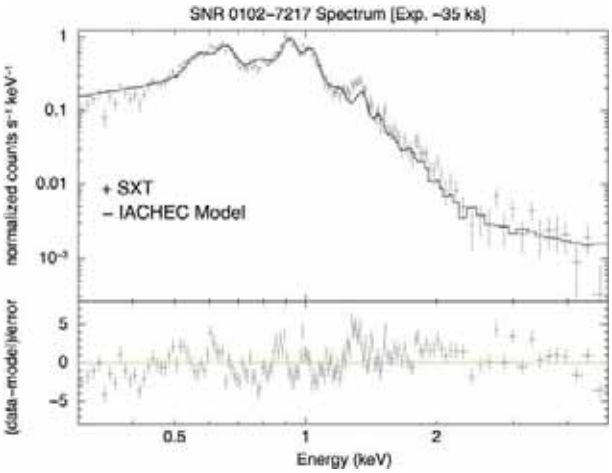

Figure 12. The X-ray spectrum of 1E0102-72.3 as fitted with the IACHEC model derived from several X-ray observatories carrying a CCD camera in the focal plane of a telescope. The SXT spectrum was extracted from a radius of 10 arcmin.

9. Conclusion

We have provided an overview of the SXT instrument and preliminary details of its in-orbit performance. SXT has observed several interesting targets and data are being analysed. The results of these observations will be reported in the literature. Further details of the X-ray optics, point spread function, vignetting, spectral response, etc. of the instrument will be presented elsewhere.

Acknowledgements

The Tata Institute of Fundamental Research (TIFR), Mumbai, led the effort with instrument design, development, integration and testing of the SXT. The Space Research Centre of the University of Leicester, UK, led the development of the Focal Plane Camera for which the processing electronics was built at TIFR. Vikram Sarabhai Space Centre, Thiruvananthapuram provided the CFRP tubular structures for the SXT. The door mechanism for the telescope, the radiator plate and the heat pipe were developed at the ISRO Satellite Centre, Bengaluru. The Space Application Centre (SAC), Ahmedabad, TIFR, Mumbai and IUCAA, Pune jointly developed the analysis software. A vast number of industries participated in the fabrication of infrastructure and mechanical components of the SXT. ISRO funded, managed and facilitated the project. Various softwares including Python, IDL, FTOOLS, C and C++ were also used.

References

Burrows D. N., Hill, J. E., Nousek, J. A. *et al*. 2005, *Space Sci. Rev.*, **120**(**3-4**), 165.

Harrison, F. A., Craig, W. W., Christensen, F. E. *et al*. 2013, *Astrophys. J.*, **770**, 103.

Kothare, A., Mirza, I., Singh, K. P., Abbey, A. F. 2009, *Nucl. Instrum. Methods Phys. Res. A*, **604**, 747.

Kunieda, H., Ishida, M., Endo, T. *et al*. 2001, *Appl. Opt.*, **40**, 553.

Plucinsky, P. P., Beardmore, A. P., Foster, A. *et al*. 2016, arXiv:1607.03069.

Rao, A. R., Patil, M. H., Bhargava, Y. *et al*. 2016, *J. Astrophys. Astron.*, this issue.

Romano, P., Cusumano, G., Campana, S. *et al*. 2005, *Proc. SPIE*, **5898**, 369R.

Sagdeo, A., Rai, S. K., Lodha, G. S. *et al.* 2010, *Exp. Astron.*, **28**, 11.

Singh, K. P., Stewart, G. C., Chandra, S. *et al*. 2016, *Proc. SPIE*, **9905**, 99051E.

Singh, K. P., Tandon, S. N., Agrawal, P. C. *et al*. 2014, *Proc. SPIE*, **9144**, 91441S.

Westergaard, N. J., Byrnak, B. P., Christensen, F. E., Grundsoe, P., Hornstrup, A. 1990, *Opt. Eng.*, **29**, 658.